12-12-2022

Proposal for a definitive search for GUT-scale QCD axions

L. Brouwer

S. Chaudhuri

H. M. Cho

J. Corbin

C. S. Dawson

See next page for additional authors

Authors

L. Brouwer, S. Chaudhuri, H. M. Cho, J. Corbin, C. S. Dawson, A. Droster, J. W. Foster, J. T. Fry, P. W. Graham, R. Henning, K. D. Irwin, F. Kadribasic, Y. Kahn, A. Keller, R. Kolevatov, S. Kuenstner, A. F. Leder, D. Li, J. L. Ouellet, K. M. W. Pappas, A. Phipps, N. M. Rapidis, B. R. Safdi, C. P. Salemi, M. Simanovskaia, J. Singh, E. C. van Assendelft, K. van Bibber, K. Wells, L. Winslow, W. J. Wisniewski, and Betty A. Young

Proposal for a definitive search for GUT-scale QCD axions

L. Brouwer,[1] S. Chaudhuri ,[2,*] H.-M. Cho,[3] J. Corbin,[4] C. S. Dawson,[4] A. Droster,[5] J. W. Foster,[6] J. T. Fry ,[7]
P. W. Graham,[4] R. Henning,[8,9] K. D. Irwin,[4,3] F. Kadribasic,[4] Y. Kahn,[10] A. Keller,[5] R. Kolevatov,[2]
S. Kuenstner,[4] A. F. Leder,[5,11] D. Li,[3] J. L. Ouellet,[7] K. M. W. Pappas,[7] A. Phipps,[12] N. M. Rapidis,[4] B. R. Safdi,[13]
C. P. Salemi ,[7,14,3,†] M. Simanovskaia,[4] J. Singh,[4] E. C. van Assendelft,[4] K. van Bibber,[5] K. Wells,[4]
L. Winslow,[7] W. J. Wisniewski,[3] and B. A. Young[15]

(DMRadio Collaboration)

[1]*Accelerator Technology and Applied Physics Division, Lawrence Berkeley National Laboratory,
Berkeley, California 94720, USA*
[2]*Department of Physics, Princeton University, Princeton, New Jersey 08544, USA*
[3]*Stanford Linear Accelerator Center, Menlo Park, California 94025, USA*
[4]*Department of Physics, Stanford University, Stanford, California 94305, USA*
[5]*Department of Nuclear Engineering, University of California, Berkeley, Berkeley, California 94720, USA*
[6]*Center for Theoretical Physics, Massachusetts Institute of Technology,
Cambridge, Massachusetts 02139, USA*
[7]*Laboratory of Nuclear Science, Massachusetts Institute of Technology,
Cambridge, Massachusetts 02139, USA*
[8]*Department of Physics and Astronomy, University of North Carolina,
Chapel Hill, Chapel Hill, North Carolina, 27599, USA*
[9]*Triangle Universities Nuclear Laboratory, Durham, North Carolina 27710, USA*
[10]*Department of Physics, University of Illinois at Urbana-Champaign, Urbana, Illinois 61801, USA*
[11]*Physics Division, Lawrence Berkeley National Laboratory, Berkeley, California 94720, USA*
[12]*California State University, East Bay, Hayward, California 94542, USA*
[13]*Department of Physics, University of California, Berkeley, Berkeley, California 94720, USA*
[14]*Kavli Institute for Particle Astrophysics and Cosmology, Stanford University, Stanford, California 94305, USA*
[15]*Department of Physics, Santa Clara University, Santa Clara, California 95053, USA*

The QCD axion is a leading dark matter candidate that emerges as part of the solution to the strong *CP* problem in the Standard Model. The coupling of the axion to photons is the most common experimental probe, but much parameter space remains unexplored. The coupling of the QCD axion to the Standard Model scales linearly with the axion mass; therefore, the highly motivated region 0.4–120 neV, corresponding to a GUT-scale axion, is particularly difficult to reach. This paper presents the design requirements for a definitive search for GUT-scale axions and reviews the technological advances needed to enable this program.

I. INTRODUCTION

There is overwhelming evidence that most of the matter in the Universe is not included in the Standard Model (SM) of particle physics [1,2]. Despite extensive theoretical and

*sc25@princeton.edu
†salemi@stanford.edu

experimental work over the past several decades, the identity of the dark matter (DM) remains unknown. One of the leading DM candidates at present is the quantum chromodynamics (QCD) axion. The axion is a light boson that was originally postulated as part of the solution to another prominent open question in particle physics, the strong *CP* problem [3–6], related to the nonobservation of a neutron electric dipole moment.

The QCD axion is the pseudo-Goldstone boson associated with the breaking of a new global $U(1)$ symmetry, called the Peccei-Quinn (PQ) symmetry, in the early Universe [7] at a high energy scale f_a. Due to its coupling to QCD, the axion gains a potential at energies below the

QCD confinement scale, leading to the axion having mass $m_a \approx 5.7(10^{15} \text{ GeV}/f_a)$ neV [8]. The axion mixes with the neutral pion to acquire a dimension-five coupling with electromagnetism of the form $\mathcal{L} \supset g_{a\gamma\gamma} a \mathbf{E} \cdot \mathbf{B}$, with $\mathbf{E}$ and $\mathbf{B}$ the electric and magnetic fields, respectively, though ultraviolet contributions to the axion-photon coupling may also be present [7,9–12]. The axion-photon coupling is $g_{a\gamma\gamma} = C_{a\gamma\gamma}\alpha_{\text{EM}}/(2\pi f_a)$, where α_{EM} is the fine-structure constant and $C_{a\gamma\gamma}$ is a constant typically of order unity that depends on the ultraviolet theory; in the DFSZ model [11,12] (KSVZ model [9,10]) $C_{a\gamma\gamma} \sim 0.75$ ($C_{a\gamma\gamma} \sim -1.92$), though some axion models achieve $|C_{a\gamma\gamma}| \gg 1$ [13–15]. The existence of a nonzero axion-photon coupling is entirely generic due to the low-energy contribution from pion mixing. Therefore, the photon coupling is a promising handle with which to search for the QCD axion.

Theoretical work has shown that axions over a wide range of masses, $m_a \in [10^{-12}, 10^{-2}]$ eV, can make up all of the DM [16–23]. Theoretical priors disfavor masses below this range, which would require super-Planckian f_a, as well as higher masses, which are in conflict with stellar cooling observations [24–28]. The preferred mass to allow axions to make up all of the DM depends on the relative timing of PQ symmetry breaking and inflation. If the PQ symmetry is broken after inflation, the axion mass that yields the observed DM abundance is expected to be $m_a \sim \mathcal{O}(100 \ \mu\text{eV})$ [29–31]. If instead the PQ symmetry is broken before inflation, then much lighter axion masses are possible through mechanisms including anthropic selection [19,20], late-time entropy dilution [21], and inflationary dynamics [22,23]. A particularly well-motivated part of this lower mass range is $m_a \sim 1–100$ neV, which corresponds to f_a near the grand unified theory (GUT) scale. Axion decay constants $f_a \sim 10^{14} - 10^{16}$ GeV arise naturally in the context of string theory constructions (see, e.g., [32–38]), which generically produce PQ symmetries through the compactification of the extra dimensions [39], and GUT field theories [21,40–46]. At these low masses, the axion Compton wavelength in our Galaxy is large relative to the size of a detector, which has motivated experiments that use lumped-element circuits to detect axion-photon interactions [47–50]. This detection technique exploits axion interactions with a static magnetic field by inductively coupling the resulting effective current into an LC circuit. Three first-generation lumped-element experiments, ABRACADABRA-10 cm, SHAFT, and ADMX-SLIC, have recently set world-leading limits [51–54].

Current results with this method are several orders of magnitude less sensitive than would be necessary to detect QCD axions at neV masses, but there are efforts underway to build more sensitive lumped-element detectors. DMRadio is a program of experiments that aims to incrementally improve the sensitivity of the lumped-element technique [55,56]. The first of these experiments is DMRadio-50L, which aims to search for axionlike particles over a wide range of

masses with couplings $g_{a\gamma\gamma} < 10^{-14}$ GeV^{-1} and is currently being constructed. A larger, more sensitive detector DMRadio-m^3 will probe $\sim$120–800 neV axions at DFSZ sensitivities [12,57].

This paper presents the path toward detecting QCD axions at GUT-motivated masses, focusing on the technology development needed to enable such a search. Achieving the required sensitivity necessitates improvements in several of the core components of the experiment: magnet, cryogenics, amplifier, and resonator. We begin in Sec. II by describing the lumped-element detection method and presenting the scan rate, which we use to set the performance required for these core components. Section III discusses the requirements on the magnet and cryogenic systems and potential paths for improvement in these areas. Section IV presents the need for beyond-standard quantum limit (SQL) amplifiers, and Sec. V describes improvements that can be made to the tunable resonator. We conclude in Sec. VI by comparing different experiment configurations that could definitively search for QCD axions in the 0.4–120 neV mass range (corresponding to rest-mass frequencies $\nu_a = m_a c^2/h$ of 100 kHz–30 MHz), probing masses associated with the GUT scale.

II. LUMPED-ELEMENT DETECTION

The axion is a type of classical wavelike DM because its small mass and consequently large number density lead to high occupation numbers per quantum state. This is in contrast to the particlelike interactions probed in searches for heavier DM candidates [58–60]. At $m_a \sim 1$ neV, the axion's Compton wavelength is $\sim$1 km, which is much larger than any current or planned DM experiment. In this regime, the magnetoquasistatic approximation holds, and the variation in the electric field associated with the axion-photon interaction is small. The axion-photon interaction can then be interpreted in terms of an axion-modified Ampère's law,

$$\nabla \times \mathbf{B} = -g_{a\gamma\gamma}\sqrt{\frac{\hbar\epsilon_0}{c}}\left(\mathbf{E} \times \nabla a - \frac{\partial a}{\partial t}\mathbf{B}\right), \qquad (1)$$

where a is the axion field. Here, we have neglected to include the displacement current term, $\partial \mathbf{E}/\partial t = 0$, (being in the magnetoquasistatic limit) or other current sources [49,61]. For cold dark matter, the spatial gradient of the axion is expected to be small relative to its time derivative, so we take as our signal only the second term on the right-hand side, which can be written as an effective current that is proportional to the magnetic field that sources the axion interactions,

$$\mathbf{J}_{\text{eff}} = \frac{\sqrt{\hbar c}}{\mu_0} g_{a\gamma\gamma}\sqrt{2\rho_{\text{DM}}}\cos(m_a t)\mathbf{B}, \qquad (2)$$
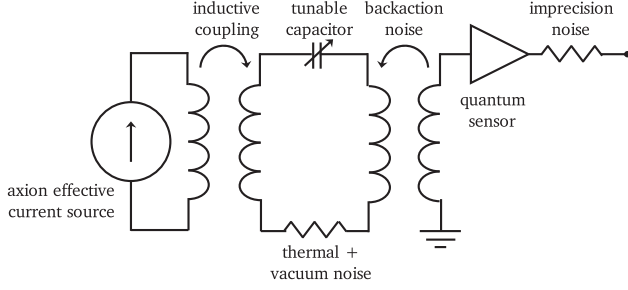
FIG. 1. Effective circuit diagram for a lumped-element axion experiment. On the left, the axions' interaction with a strong magnetic field creates an effective current source that can be inductively coupled to a superconducting circuit. The central loop acts as an LC resonator with quality factor Q, which can enhance signals that match the resonance frequency. To scan over a range of axion masses, the capacitor is tuned. Finally, the signal is read out using high-precision quantum sensors and analyzed offline. Noise enters the system in the resonator as thermal and vacuum noise and on the readout as amplifier-added noise.

where $\rho_{DM} \approx 0.45$ GeV/cm^3 is the local energy density of axion DM [62].

Using the magnetoquasistatic approximation, the axion effective current, $\mathbf{J}_{eff}$, produces oscillating magnetic fields that can be inductively coupled to a detection circuit consisting of inductors and capacitors [49], as shown in Fig. 1. This is the lumped-element circuit model from which the detection method takes its name. The signal from an axion of mass m_a is resonantly enhanced if its corresponding frequency is close to the circuit's LC resonance. Because we do not know m_a *a priori*, the LC resonance must be tuned over a wide range of frequencies. The time spent at each frequency determines the experiment's scan rate.

A. Sensitivity

The overall sensitivity of axion experiments can be evaluated in terms of their scan rate, which quantifies how quickly a detector can be sensitive to a given value of $g_{a\gamma\gamma}$ over a range of axion masses. The rate at which the resonance frequency, ν_r, is tuned is (see the Appendix for a derivation)

$$\frac{d\nu_r}{dt} \approx 41 \frac{\text{kHz}}{\text{year}} \left(\frac{3}{\text{SNR}}\right)^2 \left(\frac{g_{a\gamma\gamma}}{10^{-19} \text{ GeV}^{-1}}\right)^4 \left(\frac{\rho_{DM}}{0.45 \text{ GeV/cm}^3}\right)^2$$
$$\times \left(\frac{\nu_r}{100 \text{ kHz}}\right) \left(\frac{c_{PU}}{0.1}\right)^4 \left(\frac{B_0}{16 \text{ T}}\right)^4 \left(\frac{V}{10 \text{ m}^3}\right)^{10/3} \left(\frac{Q}{2 \times 10^7}\right) \left(\frac{10 \text{ mK}}{T}\right) \left(\frac{0.1}{\eta_A}\right). \quad (3)$$

This scan rate depends on the desired signal-to-noise ratio (SNR) on resonance for a given coupling, $g_{a\gamma\gamma}$, as well as the bandwidth over which that SNR is approximately constant, which we will refer to here as the sensitivity bandwidth. The SNR essentially determines how long the experiment must integrate at each frequency step, and the sensitivity bandwidth sets the minimum spacing between steps.

The first line in Eq. (3) contains the axion and DM physics, where we have assumed that the DM distribution follows the standard halo model (SHM) [63]. The second line describes experimental parameters: c_{PU}^2 is a proxy for the ratio of energy that is coupled into the resonant circuit to energy stored in axion-generated magnetic field. It is analogous to the form factor in a cavity axion experiment [64]. A typical value is $c_{PU} \sim 0.1$ [65]. B_0 is the peak strength of the dc magnetic field assuming a toroidal magnet with a ratio of outer to inner radii $r_{out}/r_{in} = 2$. V is the total volume of the pickup structure; see the Appendix for a discussion on the parametric dependence of scan rate on volume. Q is the quality factor of the resonant circuit. The last two terms represent thermal noise (scaling with temperature T) and amplifier noise (η_A). Note that we have assumed that thermal noise dominates over amplifier noise, as is true at the low frequencies this method searches.

As evident from Eq. (3), the most effective ways of increasing the scan rate and hence overall sensitivity are to increase the magnetic field strength and volume as well as the detector-axion coupling, c_{PU}, which scale with high powers. However, as we discuss below, order(s) of magnitude improvement may also be made to Q and η_A. The developing technologies that can facilitate these improvements are discussed in Secs. III–V and summarized in Table I.

TABLE I. R&D thrusts for improving the sensitivity of future lumped element experiments. The target values shown are those we assume for our baseline scenario of a 6.2 year scan.

Technology	Parameter(s) affected	Target value
Magnets		
REBCO magnets	B_0, V	16 T, 10 m^3
Nb$_3$Sn magnets		
Backaction evasion		
rf quantum upconverters	η_A	−20 dB
Resonators		
Passive resonators	Q	20×10^6
Active feedback		

B. Predecessor experiments

The lumped-element technique for axion detection has been demonstrated by several experiments. The first experiment to set limits using this technique was ABRACADABRA-10 cm, using a 1 T, ~1 L toroidal magnet coupled to a broadband readout circuit [66–68]. The SHAFT experiment used ferromagnets in a double-toroid configuration to also set limits in the mass range near 1 neV [69].

The experiment ADMX-SLIC used a different configuration to look for axions at slightly higher masses [70]. A solenoidal magnet provided a strong field (up to 7 T) for the axions to couple to, and the resulting signal was read out via a tunable resonant circuit. The DMRadio-Pathfinder dark photon search also demonstrated the use of a tunable resonant readout, although without the magnetic field that is required for axion searches [71].

Using this lumped-element method, each of these small experiments was able to search for axions in unexplored $g_{a\gamma\gamma}$ parameter space. They demonstrated long-term operation and data-taking stability, successful resonator tuning at cryogenic temperatures, and the ability to integrate a tesla-scale magnetic field in conjunction with a sensitive superconducting readout. Upcoming experiments will address the challenges encountered by these prototype detectors, including the isolation of vibrational and other environmental noise sources and the development and maintenance of a high-Q tunable resonator.

The central objective for future experiments is improving sensitivity to $g_{a\gamma\gamma}$ as dictated by the scan rate in Eq. (3). The next experiment to use the lumped-element technique, DMRadio-50L, focuses on improving the axion-detector coupling, increasing the science volume, and implementing a resonant readout. The experiment will have a toroidal ~50 L magnetic field volume and will significantly improve the coupling factor by enclosing the axion effective current in a superconducting pickup sheath. This new pickup will also allow the experiment to use a resonator with a Q-factor of ~10^6 [72,73]. The DMRadio-m^3 experiment will further scale up the magnetic field and volume (with a solenoidal topology), improving the sensitivity enough to search for DFSZ axions at slightly higher masses.

The DMRadio-50L and DMRadio-m^3 experiments will be able to provide insight into the potential challenges in construction, integration, and operation of DMRadio-GUT at a larger scale than was achieved by the prototype experiments. For example, we expect to learn more about the feasibility of cooling and operating a massive magnet in tandem with highly sensitive superconducting electronics. DMRadio-GUT will combine these lessons with upcoming technological advances in order to achieve the exquisite sensitivities necessary for a successful GUT-scale experiment. In the following sections we lay out the R&D path towards this goal.

III. MAGNET AND CRYOGENICS

The predecessor experiments use one of two basic geometries: a toroidal or solenoidal magnet. The toroidal design has some major advantages. In a toroid, the magnetic field is contained within the coils, unlike a solenoidal field with field lines that return outside of the magnet bore. Magnet quenches are thus much less dangerous and also pose minimal threat to the superconducting electronics, which need to operate in a low-field region. Contained fields also allow the pickup structure to naturally sit in a field-free location. This placement avoids introducing leading-order magnet-related backgrounds into the readout, and it also allows the pickup to be easily constructed from superconducting materials, leading to higher resonator Q's. However, the pickup geometries used in toroidal designs suffer from parasitic resonances (due to capacitance in overlapping sheath components), which can limit their sensitivity at high frequencies. Because DMRadio-GUT is designed for low frequency, the issue of parasitic resonances for a toroidal architecture is mitigated.

In the solenoidal design, the pickup is most sensitive when inside the high field region. However, this placement increases the risk of magnet-sourced noise, and large fields make the construction of a high-Q circuit difficult [74]. High-field solenoids are produced for many applications, so they benefit from existing designs and infrastructure for their construction. They are thus generally easier and cheaper to build.

Experience from the toroidal DMRadio-50L and solenoidal DMRadio-m^3 experiments will be important inputs into the decision of DMRadio-GUT 's geometry. For example, magnetic pinning effects in the solenoidal field could reduce vibrational noise, making that design more competitive, especially if vibrations are a dominant noise source [75]. Simulations and measurements of the DMRadio-m^3 detector will guide our estimates of the importance of vibrational backgrounds in a potential solenoidal DMRadio-GUT. Likewise, we will be able to measure any stray fringe fields from the DMRadio-50L toroid that can produce interference and vibrational noise in the pickup and use that to gauge tolerances on the construction of a DMRadio-GUT toroid. Ultimately, we expect that in a solenoid, the disadvantages of the pickup being in the high-field region would be a limitation, making the toroidal design the most likely outcome.

Regardless of the geometry, the DMRadio-GUT magnet will have to be large and thus heavy. As in DMRadio-50L and DMRadio-m^3, we plan to cool only the resonator to sub-K temperatures. However, even with the goal of cooling the magnet only to its superconducting transition temperature, T_c, careful consideration will have to be made in the design of the cryogenics. For the toroidal design, some of the cryogenic constraints are mitigated by surrounding the magnet with a superconducting sheath, as in DMRadio-50L, which ensures that the resonator does not

couple to magnet loss or thermal noise that would otherwise degrade sensitivity. The primary decision that will determine the cryogenic requirements is the choice of magnet wire materials, which can be grouped into two categories, traditional, low-T_c superconductors and newer, high-T_c superconductors such as rare earth barium copper oxides (REBCO).

A. Low-T_c magnet

There are many low-T_c superconductors, but generally Nb-based compounds are favored for the construction of high field magnets. Here we explore two common choices that could be used in DMRadio-GUT.

The first option is to use a traditional NbTi superconducting magnet, as has been done for the other lumped-element detectors. A NbTi-based design would require cooling the magnet below 10 K and would also limit the peak magnetic field strength to ~10 T [76], posing stringent practical constraints on DMRadio-GUT. In order to maintain our goal sensitivity, this restriction on field strength would require greatly increasing the magnet volume, which would further increase the load on the cryogenics and/or require large improvements in the noise and quality factor of the receiver.

A second option is to use a Nb$_3$Sn magnet. While more costly and difficult to use in magnet fabrication, Nb$_3$Sn can produce the benchmark 16 T magnetic field for a GUT-scale QCD axion search. Significant work has been done in related fields to optimize use of Nb$_3$Sn magnets in large-scale physics experiments. For example, the ITER fusion project will utilize solenoidal and toroidal Nb$_3$Sn coils operating at a temperature of ~5 K with peak fields of 13 T and 11.8 T, respectively [77]. The latter toroidal magnets, used for confining the plasma, will have 8500 m^3 volume and 51 GJ of stored energy. This material will also be used as part of the High-Luminosity LHC, for the accelerator's dipole and quadrupole magnets, reaching 12 T peak fields and 2.5 GJ of stored energy [78,79].

B. High-T_c magnet

Additional options beyond low-T_c magnets are on the horizon due to recent and emerging advancements in high temperature superconducting (HTS) materials. HTS-based magnets have several advantages over traditional niobium-alloy-based magnets. First, because of the higher T_c, the cooling requirements for the large magnet mass can be relaxed; HTS magnets can operate at a few tens of kelvin instead of a few kelvin. Second, HTS materials such as REBCO are able to remain superconducting in fields exceeding 35 T [80], allowing us to increase B_0 and provide additional engineering margin for a GUT-scale search.

HTS magnets are already being used for a variety of projects, most notably in fusion, which, similar to DMRadio-GUT, requires high fields and large volumes. One such project is the SPARC tokamak [81], a toroidal

magnet made of YBCO tape with an average magnetic field of 12.2 T and a major radius of 1.85 m for a total stored energy of 110 MJ. Recently, the SPARC effort demonstrated peak fields of 20 T.

By taking advantage of these developments in magnet technology, lumped-element experiments can greatly improve their reach. DMRadio-GUT plans to achieve a 12 T root-mean-square (RMS) field (equivalent to a 16 T peak field for a toroid with the same approximate aspect ratio as DMRadio-50L) in a 10 m^3 volume, for a total stored energy of 573 MJ, well within the bounds of current and planned magnets. However, even with these magnet parameters, running the experiment with SQL amplifiers would require a runtime of ~50 years. A powerful magnet will consequently need to be paired with beyond-SQL amplifiers, as we explore in the next section.

IV. BEYOND-SQL AMPLIFIERS

Simultaneous with the explosion in interest in wavelike axion DM, there has been a revolution in quantum sensing, enabling measurements at unprecedented sensitivity. These new capabilities will facilitate searches for QCD axions over a much wider parameter space.

There are two primary requirements on quantum sensors for axion searches. First, they must be sensitive to tiny signals, since a receiver couples a miniscule amount of power from the axion field [65] (e.g., $\lesssim 10^{-22}$ W for traditional cavity-based DFSZ axion searches in several-tesla magnetic fields [75]). Second, because the axion mass is unknown, measurements must be able to scan over orders of magnitude in frequency. Thus, usable sensors must not only enable a high SNR, but they must also be able to do so over a wide bandwidth in frequency in order to increase step sizes and achieve a fast scan. As described in Ref. [65] (see also Sec. VI B of [82] and [83] for an extended discussion), the figure of merit for readout sensors is thus a frequency-integrated sensitivity, increasing with both the on resonance SNR and the bandwidth over which that SNR can be maintained.

Progress has already been made towards implementing beyond-SQL measurement in axion searches in the microwave frequency range ($\gtrsim 1$ GHz). The HAYSTAC experiment has demonstrated an axion receiver in which the cavity is injected with squeezed electromagnetic vacuum, doubling the bandwidth and consequently the experiment's scan rate over previous work [84]. Recent work on qubit-based photon counting has demonstrated a noise reduction that could yield a factor of 1,300 increase in scan rate compared to a quantum-limited search [85].

To enable DMRadio-GUT, we must develop quantum sensing technologies at much lower frequencies, in the range of 1 kHz–100 MHz. Unlike the upper end of the microwave frequency range (the green region in Fig. 2), at the frequencies of a GUT-scale axion, the resonator is thermally occupied, which means that quantum noise-evading
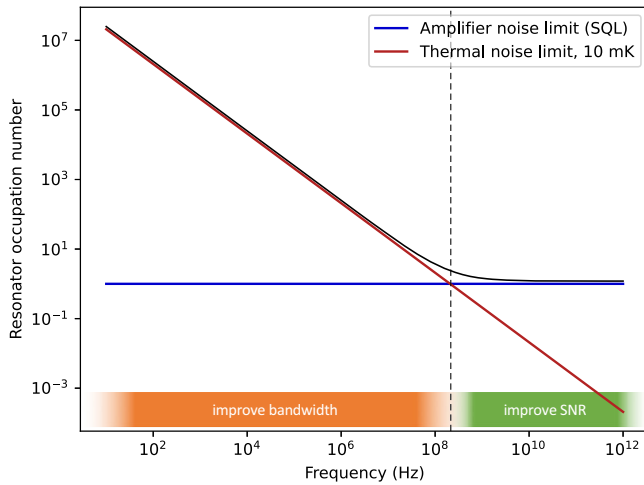
FIG. 2.   There are two distinct noise regimes in axion searches. At high frequencies, thermal noise is subdominant to readout noise, and so improvements in readout performance beyond the SQL directly improve the SNR. At low frequencies, thermal noise is dominant, and so beyond-SQL amplification does not directly improve the SNR. Instead, integrated sensitivity can be improved by increasing the sensitivity bandwidth.

techniques such as squeezing or photon counting do not significantly improve SNR relative to a quantum-limited readout. The objective in this range (Fig. 2's orange region) is thus to improve the frequency-integrated sensitivity by executing quantum protocols on thermal states to increase the bandwidth rather than the SNR [86,87].

At our low frequencies, with a quantum-limited amplifier, resonator thermal noise dominates quantum noise over a broad range of frequencies much larger than the resonator bandwidth. Over this range of thermal noise domination, the SNR is approximately constant because the resonator response to the signal and noise are identical—they both vary with frequency approximately as Lorentzian functions. This range over which the SNR is constant is what we call the "sensitivity bandwidth," because we are equally sensitive to an axion signal throughout, even in the region outside the resonator bandwidth. To enhance scan sensitivity with a quantum sensing protocol, it is then natural to increase the sensitivity bandwidth.

As illustrated in Fig. 3, a backaction evasion scheme both reduces the minimum added noise of the readout below the one-photon SQL and increases the sensitivity bandwidth. The bandwidth improvement relies on the fact that the amplifier noise can be divided into two components with different inherent line shapes; see the Appendix, Sec. V of [87], and Appendix F of [82] for more information. The first component, known as imprecision noise, is a flat background that is added on the amplifier output. The second component is backaction, which is injected back into the detector resonator through the amplifier input. Because it goes through the resonator, backaction shares the resonator's Lorentzian line shape. For

an example of how this works, we can examine dc superconducting quantum interference device (SQUIDs), which have demonstrated noise as low as 20 times the quantum limit in commercial implementations [88] and which are the baseline for DMRadio-50L and DMRadio-m^3. In SQUIDs, the imprecision noise consists of intrinsic voltage fluctuations on the amplifier output, and the backaction noise consists of circulating currents in the SQUID loop, which induce a voltage and thus resonantly enhanced currents in the input coil [89,90].

The sum of the imprecision and backaction components is the total amplifier noise plotted in Fig. 3, and it is this sum that is subject to the SQL. By tuning the strength of the input coupling of the amplifier, one can adjust the balance of imprecision versus backaction noise. Improvement on this scheme can be accomplished with backaction evasion, shown in the bottom row of Fig. 3, where the backaction in one quadrature of the signal is reduced at the expense of increased backaction in the other quadrature. As in the top row, by coupling the amplifier more strongly to the readout, the imprecision noise is reduced, increasing backaction noise—but now only in the unmeasured quadrature. This process thus maintains the noise levels of the measured backaction quadrature and lowers the imprecision noise, increasing the sensitivity bandwidth.

An alternative approach to backaction evasion is variational readout. For amplifiers subject to the SQL, the imprecision and backaction noise are uncorrelated. By introducing correlations between the imprecision and backaction, one can achieve a better noise match and reduce the total noise off resonance, thereby increasing the sensitivity bandwidth. The introduction of correlations to reduce off resonance noise has been demonstrated in microwave measurements of mechanical resonators [91].

One possibility for implementing these quantum protocols for 1 kHz–100 MHz electromagnetic signals is the rf quantum upconverter (RQU); see also Chaps. 6 and 7 of [92] as well as [93] and [94]. Like a dc SQUID, the RQU takes a flux signal as its input, which facilitates its integration as an upgrade to the DMRadio readout chain. However, in contrast to a dc SQUID, for which the input and output signals match in frequency, the RQU upconverts kHz–MHz flux signals to GHz voltage signals, allowing us to leverage existing microwave quantum technologies [95]. The RQU is realized by embedding an interferometer of Josephson junctions in a superconducting microwave resonator. This setup implements a measurement Hamiltonian analogous to that of cavity optomechanics, where decades of work has enabled quantum sensing on low-frequency, mechanical systems (e.g., LIGO) [96,97]. RQUs can thus use analogous protocols for quantum noise-evasion, such as the backaction evasion scheme proposed for mechanical resonators in [98]; in an RQU, this scheme may be executed by exciting the microwave resonator with an amplitude-modulated drive.

By implementing quantum protocols, we aim to achieve readout noise levels of $\eta_A = 0.1$, corresponding to 20 dB of
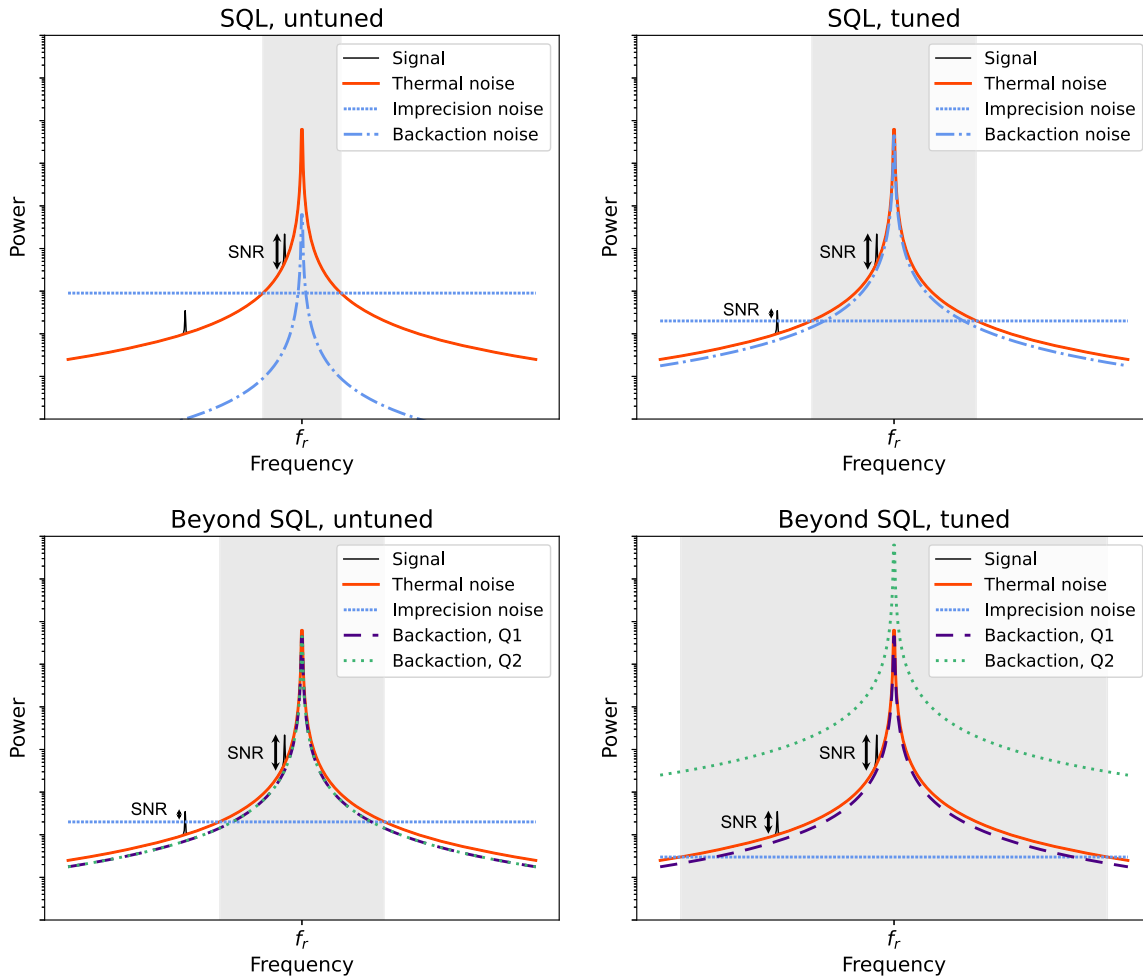
FIG. 3.   Optimizing the sensitivity bandwidth for quantum-limited amplification, top, and beyond-SQL amplification via backaction evasion, bottom. The cases with untuned amplifier input coupling are on the left, and the more optimally coupled cases are shown on the right. Note that the SNR (labeled in black) is similar for the near-resonance signal in each case while the sensitivity bandwidth (grey band) can be greatly increased by tuning the coupling. A second, off resonance signal is shown, buried under the noise for an untuned, SQL setup. By tuning the coupling, the signal may rise above the amplifier noise, and in the final, tuned beyond-SQL case, it can reach its maximum SNR above the thermal noise background. Using beyond-SQL amplifiers allows the experimenter to shift more of the imprecision noise into backaction without affecting the SNR of signals in the sensitivity bandwidth; the noise only goes into the unmeasured quadrature, here Q2.

backaction-noise reduction and a factor of 10 increase in scan rate. Quantum squeezing of 10 dB has already been achieved in the GHz regime using Josephson parametric amplifiers, and more recently, quantum squeezing of 20 dB (analogous to our goal) was demonstrated in a spin ensemble controlled by optical light [99,100]. As part of demonstrations toward DMRadio-GUT, RQUs and quantum protocols may be integrated into the DMRadio-50L test bed.

V. RESONATOR R&D

To probe GUT-scale QCD axion DM, it will be necessary to improve lumped-element resonators in the frequency range 1 kHz–100 MHz. We envision a two-pronged approach: (1) increasing the quality factor of a passive resonator and (2) implementing active matching to increase bandwidth without reducing resonator gain.

A. Passive resonator

State of the art lumped-element resonators have demonstrated quality factors of $\mathcal{O}(10^6)$ using wire-wound NbTi coils and commercial capacitors when the components are kept away from magnetic fields (as would be the case for a toroidal magnet surrounded by a pickup inductor) [72,73]. However, they possess potentially dominant loss mechanisms in the form of normal metal joints and dielectric loss in polytetrafluoroethylene (PTFE) and formvar wire coatings. Moreover, there exists only a limited understanding of what dictates quality factor in lumped-element resonators.

These issues motivate a systematic study to understand loss mechanisms with the aim of improving Q in the 1 kHz–100 MHz frequency range. A program is underway to explore the use of a variety of superconductors for wires and electrodes—niobium, aluminum, titanium, tantalum, and their alloys—and crystalline capacitor dielectrics for frequency tuning–sapphire, silicon, rutile. Through careful experimental study and optimization of Q, superconducting radio frequency cavities in the GHz range have demonstrated Qs on the order of 10^{12} (one million times higher than lumped-element resonators) [101]. The current goal is to improve Q in the 1 kHz–100 MHz frequency range by a factor of 20 to 20 million. As described below, a GUT-scale probe may also be realized with only a factor of 2 improvement in Q if sufficiently high field, HTS toroidal magnets are implemented. Resonators with improved Q may be integrated into the DMRadio-50L testbed as a demonstrator for DMRadio-GUT.

For resonator tuning structures, we plan to build upon the techniques developed for DMRadio-50L and DMRadio-m³. As described previously, the physical size of the receiver is decoupled from the search frequency; therefore, we may achieve appreciable tuning with a single resonator configuration. The resonance frequency may be tuned in the LC circuit by changing the capacitance. Simulation has indicated that we may achieve a factor of 10 change in capacitance using an insertable dielectric or a tunable electrode overlap, resulting in a factor of ∼3 in frequency change in a single cooldown. Such tuning mechanisms need not unacceptably degrade the Q; sapphire loaded superconducting cavities have demonstrated quality factors in excess of 10^9 [102]. For coarser tuning, inductor coil sets may be changed between cooldowns to scan different frequency ranges. In this manner, DMRadio-GUT can probe the desired 0.1–30 MHz frequency range with as few as five resonator configurations.

B. Active feedback

A passive resonator is not the only option for the impedance matching network that transfers the signal to the amplifier. In a passive lumped LC circuit, the reactance of the inductor and capacitor cancel at resonance. The power absorption from axions is thus maximized at that frequency but falls off away from resonance. To circumvent the limitation, one may instead use receivers with active elements [103]. For example, if the capacitor is replaced with a negative inductor with negligible loss, one may cancel the reactance and achieve the maximum power absorption over a broad range of frequencies. Such wide-band reactance-cancellation schemes would permit the evasion of the Bode-Fano criterion [65,104,105], and they have been discussed for several decades in the engineering community such as in the context of white-light cavities in the optical regime [106–108]. Moreover, near-dissipation-less negative inductors can be realized in the kHz and MHz regimes using Josephson junctions [89]. Research and development toward DMRadio-GUT will aim to exploit active matching elements as a potential route to realizing a GUT-scale axion search.

VI. REACH AND DISCUSSION

The program outlined above coupled with the success of current lumped-element searches suggests that the discovery of GUT-scale axions with DFSZ couplings is within reach. The predicted reach of the DMRadio-GUT experiment is shown in Fig. 4 using the baseline design parameters found in Table II.

DMRadio-GUT's success does not require that all R&D tasks outlined above achieve their design goals. There can be trade-offs between the performance of each of the core systems while maintaining sensitivity to DFSZ axions with
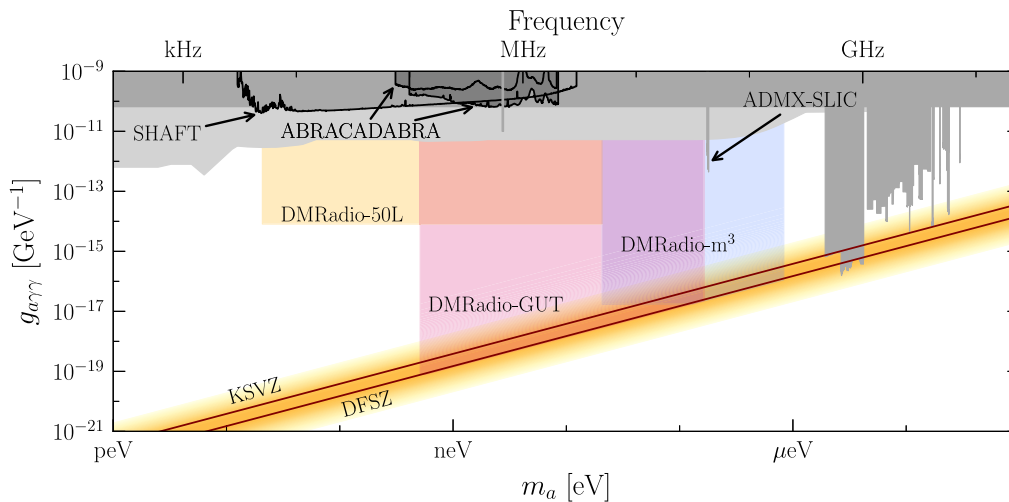

FIG. 4. Projected sensitivity for DMRadio-GUT in pink. The total scan time to cover this reach is ∼6 years, depending on R&D outcomes. Various scenarios are outlined in Table II. Existing limits are shown in grey.

TABLE II. Experimental parameters for a few different scenarios. All scenarios reach DFSZ sensitivities at SNR = 3 for $m_a \in$ [0.4, 120] neV assuming $\rho_{\mathrm{DM}} = 0.45$ GeV/cm^3. B_0 is peak field strength, V is volume of the pickup structure, c_{PU} is the strength of the detector-axion effective current coupling (described in Sec. II A), Q is the resonator quality factor, η_A is the amplifier noise, and T is the system operating temperature. The alternative scenarios in rows 2–5 explore potential detector configurations for different R&D outcomes. For example, in row 2, if amplifier R&D does not reach its goal of −20 dB of backaction-noise reduction, increasing the magnetic field strength can counteract the sensitivity reduction and result in a comparable total scan time. The total scan times in the table are calculated from Eq. (3).

Scenario	B_0	V	c_{PU}	Q	η_A	T	Scan time
Baseline	16 T	10 m^3	0.1	20×10^6	−20 dB	10 mK	6.2 years
Stronger magnet + higher noise	29 T	10 m^3	0.1	20×10^6	−5 dB	10 mK	3.2 years
Lower noise + lower volume	16 T	8 m^3	0.1	20×10^6	−25 dB	10 mK	7.3 years
Higher volume + lower Q	16 T	17 m^3	0.1	2×10^6	−20 dB	10 mK	10.6 years
Stronger magnet + lower Q	26 T	10 m^3	0.1	2×10^6	−20 dB	10 mK	8.9 years

reasonable scan times. For example, if there is difficulty reducing the sensor amplifier noise far below the SQL, then an increase in magnetic volume can compensate. A few of these scenarios are outlined in Table II. The most ambitious may be the stronger magnet with higher noise scenario. However, a 29 T peak field (20 T RMS) magnet is still within the R&D goals of the greater magnet community [109–111].

A definitive search for axion DM across all masses is one of the highest priorities for particle physics and key to uncovering the particle nature of DM [112]. Lumped-element detection is the low-frequency complement to experiments searching at higher masses. The DMRadio-GUT experiment laid out here is designed to address parameter space in the mass range 0.4–120 neV (0.1–30 MHz), probing axions at the GUT scale. It is the ultimate experiment for the lumped-element technique, harnessing key technological advancements to probe this critical parameter space.

ACKNOWLEDGMENTS

APPENDIX: SCAN RATE

Here we present a sketch of a parametric derivation for the scan rate of a resonant lumped-element experiment. This is meant to provide intuition for this kind of system rather than being a rigorous derivation for a detector setup; for the latter, see [82].

Starting with the standard Dicke radiometer equation for the SNR, we have

$$\mathrm{SNR} = \frac{P_{\mathrm{sig}}}{P_n} \sqrt{\Delta \nu_{\mathrm{sig}} \cdot \tau}, \tag{A1}$$

where τ is the integration time and $\Delta \nu_{\mathrm{sig}}$ is the signal bandwidth. For a low-frequency lumped-element receiver read out by a flux-to-voltage amplifier (e.g., a SQUID), such as DMRadio, we are not measuring a power at the amplifier input but a current. Moreover, the amplifier input is predominantly reactive instead of dissipative, in contrast to the amplifiers used in cavity experiments such as ADMX and HAYSTAC. The appropriate expression for SNR in DMRadio is then given by replacing power with the squared modulus of the corresponding currents,

$$\mathrm{SNR} = \frac{|I_{\mathrm{sig}}|^2}{|I_n|^2} \sqrt{\Delta \nu_{\mathrm{sig}} \cdot \tau}. \tag{A2}$$

From this, we would like to derive the resonator scan rate, given by

$$\frac{d\nu_r}{dt} \sim \frac{\Delta \nu_{\mathrm{sens}}}{\tau}. \tag{A3}$$

$\Delta\nu_{\text{sens}}$ is the so-called sensitivity bandwidth (also sometimes termed "visibility bandwidth"), the bandwidth over which a constant SNR can be maintained. τ is again an integration time, where it is now specifically the time required to achieve a given SNR in the sensitivity bandwidth.

Rearranging Eq. (A2) gives us the scan rate,

$$\frac{d\nu_r}{dt} \sim \frac{\Delta\nu_{\text{sens}}}{\tau} = \frac{\Delta\nu_{\text{sens}}\Delta\nu_{\text{sig}}}{\text{SNR}^2} \frac{|I_{\text{sig}}|^4}{|I_n|^4}. \tag{A4}$$

We will now step through each component of the Eq. (A4) to give the scan rate in terms of experimental parameters.

The signal current is determined by the strength of the axion effective current and its coupling into the resonant circuit. The strength of the effective current is given in (2), and the real magnetic field induced by it can be determined via Ampère's law,

$$\int \mathbf{B}_{ax} \cdot d\mathbf{l} = \mu_0 \int \mathbf{J}_{\text{eff}} \cdot d\mathbf{A}. \tag{A5}$$

Using $V^{1/3}$ as a proxy for the length scale of our system and dropping numerical factors, we have

$$|\mathbf{B}_{ax}| \sim \mu_0 |\mathbf{J}_{\text{eff}}| V^{1/3}. \tag{A6}$$

Thus the magnetic energy from the axions is

$$U_{ax} = |\mathbf{B}_{ax}|^2 V \sim \mu_0^2 |\mathbf{J}_{\text{eff}}|^2 V^{5/3}. \tag{A7}$$

Some fraction of this energy will be coupled into the readout resonator, which we parametrize by c_{PU}^2, following the convention of Sec. VI B of [82]. If the axion signal frequency matches the LC resonance frequency, the energy stored in the resonator is rung up according to the resonator quality factor, giving

$$U_{\text{sig}} \sim c_{PU}^2 Q^2 U_{ax}. \tag{A8}$$

The power dissipated in the resonator is related to the signal energy and current by

$$P_{\text{sig}} = 2\pi\nu U_{\text{sig}}/Q = \frac{1}{2}|I_{\text{sig}}|^2 R, \tag{A9}$$

where R is the equivalent-RLC resonator resistance. We thus arrive at

$$|I_{\text{sig}}|^4 \sim \frac{\nu^2}{R^2}(\hbar c)^2 (g_{a\gamma\gamma}{}^4 \rho_{\text{DM}}^2)(c_{PU}^4 Q^2 B_0^4 V^{10/3}). \tag{A10}$$

The noise current has contributions from thermal noise and amplifier-added noise, the latter of which can be further subdivided into flat imprecision noise and resonator-shaped backaction noise. Within the sensitivity bandwidth, the thermal noise dominates (see Fig. 3), so we write

$$|I_n|^4 \sim \frac{(k_B T)^2 \Delta\nu_{\text{sig}}^2}{R^2}. \tag{A11}$$

The final components of our scan rate are the signal and sensitivity bandwidths. Typically, the signal bandwidth is assumed to be identical to the axion bandwidth, but in the case where the sensitivity bandwidth is smaller than the DM bandwidth (e.g., experiments with very high Q), the signal bandwidth is instead equivalent to the sensitivity bandwidth,

$$\Delta\nu_{\text{sig}} \sim \min\left(\Delta\nu_{\text{sens}}, \frac{\nu}{Q_{\text{axion}}}\right), \tag{A12}$$

where $Q_{\text{axion}} \sim 10^6$ is the characteristic quality factor governed by the DM bandwidth.

The sensitivity bandwidth is determined by optimizing the resonator-amplifier coupling. Tuning the strength of this coupling modifies how noise is allotted between imprecision and backaction. In the limit that the physical temperature T is much larger than amplifier noise temperature T_N, the optimized sensitivity bandwidth is

$$\Delta\nu_{\text{sens}} \sim \frac{n_{\text{therm}}}{\eta_A} \Delta\nu_r. \tag{A13}$$

Here $n_{\text{therm}} \sim k_B T/h\nu_r$ is the thermal occupation number of the LC circuit, $\eta_A = 2k_B T_N/h\nu_r$ characterizes the amplifier noise, and $\Delta\nu_r = \nu_r/Q$ is the resonator bandwidth. $\eta_A = 1$ corresponds to the SQL. While a complete derivation of the optimized sensitivity bandwidth is given in Appendix F of [82], the parametrics of Eq. (A13) can readily be understood from standard noise-matching concepts [87]. In particular, the product of the imprecision and backaction noise is proportional to η_A^2.

First, suppose that the readout is noise-matched, meaning that the imprecision and backaction noise are equal on resonance. The thermal noise is $\propto n_{\text{therm}}$ and the imprecision noise is $\propto \eta_A$, so on resonance, their ratio is $\propto n_{\text{therm}}/\eta_A$. The sensitivity bandwidth is defined as the region where the thermal noise dominates over the imprecision noise; since the thermal noise follows a Lorentzian with respect to frequency, falling off as the inverse-squared at large detunings, the sensitivity bandwidth is then $\propto \sqrt{n_{\text{therm}}/\eta_A}$.

For a noise-matched amplifier, the backaction noise is $\propto \eta_A$. However, as we increase the coupling to the amplifier and the noise mismatch, the backaction noise increases, and the imprecision noise proportionally decreases. The backaction noise can thus be increased by a factor of $\sim n_{\text{therm}}/\eta_A$ up to the thermal noise $\sim n_{\text{therm}}$ without causing a degradation in on resonance SNR. Thus, at optimal coupling (which is a noise mismatch), the imprecision noise is $\propto \eta_A^2/n_{\text{therm}}$, and the ratio of thermal to imprecision noise is $\propto n_{\text{therm}}^2/\eta_A^2$. Using the same reasoning as in the noise-matched case, this results in the sensitivity bandwidth of Eq. (A13).

Rewriting gives

$$\Delta \nu_{\text{sens}} \sim \frac{k_B T}{h \eta_A Q}. \quad (A14)$$

Putting all of these pieces together, we now have a scan rate,

$$\frac{d\nu_r}{dt} \sim \frac{1}{\text{SNR}^2} (\hbar c)^2 (g_{a\gamma\gamma}{}^4 \rho_{\text{DM}}^2)(c_{PU}^4 \nu_r^2 Q^2 B_0^4 V^{10/3})$$
$$\times \left(\frac{1}{(k_B T)^2 \Delta \nu_{\text{sig}}^2}\right) \Delta \nu_{\text{sens}} \Delta \nu_{\text{sig}}, \quad (A15)$$

Assuming $\Delta \nu_{\text{sens}} > \Delta \nu_{\text{axion}}$ the rate simplifies to

$$\frac{d\nu_r}{dt} \sim Q_{\text{axion}} \frac{(\hbar c)^2}{\text{SNR}^2} (g_{a\gamma\gamma}{}^4 \rho_{\text{DM}}^2 \nu_r) \left(c_{PU}^4 \frac{Q B_0^4 V^{10/3}}{k_B T \eta_A}\right), \quad (A16)$$

which, using precise values from the SHM (see [63,113]) and integrated sensitivity optimization [see Eqs. (245) and (260) and footnote 6 of [82]], becomes Eq. (3) when parametrized by the baseline scenario values in Table II.

[1] G. Bertone, D. Hooper, and J. Silk, Particle dark matter: Evidence, candidates and constraints, Phys. Rep. **405**, 279 (2005).

[2] N. Aghanim *et al.* (Planck Collaboration), Planck 2018 results. VI. Cosmological parameters, Astron. Astrophys. **641**, A6 (2020).

[3] R. D. Peccei and H. R. Quinn, *CP* Conservation in the Presence of Instantons, Phys. Rev. Lett. **38**, 1440 (1977).

[4] R. D. Peccei and H. R. Quinn, Constraints imposed by *CP* conservation in the presence of instantons, Phys. Rev. D **16**, 1791 (1977).

[5] S. Weinberg, A New Light Boson?, Phys. Rev. Lett. **40**, 223 (1978).

[6] F. Wilczek, Problem of Strong p and t Invariance in the Presence of Instantons, Phys. Rev. Lett. **40**, 279 (1978).

[7] L. Di Luzio, M. Giannotti, E. Nardi, and L. Visinelli, The landscape of QCD axion models, Phys. Rep. **870**, 1 (2020).

[8] G. Grilli di Cortona, E. Hardy, J. Pardo Vega, and G. Villadoro, The QCD axion, precisely, J. High Energy Phys. 01 (2016) 034.

[9] J. E. Kim, Weak Interaction Singlet and Strong *CP* Invariance, Phys. Rev. Lett. **43**, 103 (1979).

[10] M. A. Shifman, A. I. Vainshtein, and V. I. Zakharov, Can confinement ensure natural *CP* invariance of strong interactions?, Nucl. Phys. **B166**, 493 (1980).

[11] M. Dine, W. Fischler, and M. Srednicki, A simple solution to the strong *CP* problem with a harmless axion, Phys. Lett. **104B**, 199 (1981).

[12] A. R. Zhitnitsky, On possible suppression of the axion hadron interactions. (In Russian), Sov. J. Nucl. Phys. **31**, 260 (1980).

[13] M. Farina, D. Pappadopulo, F. Rompineve, and A. Tesi, The photo-philic QCD axion, J. High Energy Phys. 01 (2017) 095.

[14] P. Agrawal, J. Fan, M. Reece, and L.-T. Wang, Experimental targets for photon couplings of the QCD axion, J. High Energy Phys. 02 (**2018**) 006.

[15] A. V. Sokolov and A. Ringwald, Photophilic hadronic axion from heavy magnetic monopoles, J. High Energy Phys. 06 (2021) 123.

[16] M. Dine and W. Fischler, The not so harmless axion, Phys. Lett. **120B**, 137 (1983).

[17] J. Preskill, M. Wise, and F. Wilczek, Cosmology of the invisible axion, Phys. Lett. **120B**, 127 (1983).

[18] L. F. Abbott and P. Sikivie, A cosmological bound on the invisible axion, Phys. Lett. **120B**, 133 (1983).

[19] M. Tegmark, A. Aguirre, M. Rees, and F. Wilczek, Dimensionless constants, cosmology and other dark matters, Phys. Rev. D **73**, 023505 (2006).

[20] M. P. Hertzberg, M. Tegmark, and F. Wilczek, Axion cosmology and the energy scale of inflation, Phys. Rev. D **78**, 083507 (2008).

[21] R. T. Co, F. D'Eramo, and L. J. Hall, Supersymmetric axion grand unified theories and their predictions, Phys. Rev. D **94**, 075001 (2016).

[22] P. W. Graham and A. Scherlis, Stochastic axion scenario, Phys. Rev. D **98**, 035017 (2018).

[23] F. Takahashi, W. Yin, and A. H. Guth, QCD axion window and low-scale inflation, Phys. Rev. D **98**, 015042 (2018).

[24] G. G. Raffelt, Astrophysical axion bounds, Lect. Notes Phys. **741**, 51 (2008).

[25] N. Viaux, M. Catelan, P. B. Stetson, G. Raffelt, J. Redondo, A. A. R. Valcarce, and A. Weiss, Neutrino and Axion Bounds from the Globular Cluster M5 (NGC 5904), Phys. Rev. Lett. **111**, 231301 (2013).

[26] A. Ayala, I. Domínguez, M. Giannotti, A. Mirizzi, and O. Straniero, Revisiting the Bound on Axion-Photon Coupling from Globular Clusters, Phys. Rev. Lett. **113**, 191302 (2014).

[27] P. Carenza, T. Fischer, M. Giannotti, G. Guo, G. Martínez-Pinedo, and A. Mirizzi, Improved axion emissivity from a supernova via nucleon-nucleon bremsstrahlung, J. Cosmol. Astropart. Phys. 10 (2019) 016; J. Cosmol. Astropart. Phys. 05 (2020) E01.

[28] M. Buschmann, C. Dessert, J. W. Foster, A. J. Long, and B. R. Safdi, Upper Limit on the QCD Axion Mass from Isolated Neutron Star Cooling, Phys. Rev. Lett. **128**, 091102 (2022).

[29] V. B.. Klaer and G. D. Moore, The dark-matter axion mass, J. Cosmol. Astropart. Phys. 11 (2017) 049.

[30] M. Gorghetto, E. Hardy, and G. Villadoro, More axions from strings, SciPost Phys. **10**, 050 (2021).

[31] M. Buschmann, J. W. Foster, A. Hook, A. Peterson, D. E. Willcox, W. Zhang, and B. R. Safdi, Dark matter from axion strings with adaptive mesh refinement, Nat. Commun. **13**, 1049 (2022).

[32] M. B. Green and J. H. Schwarz, Anomaly cancellation in supersymmetric $D = 10$ gauge theory and superstring theory, Phys. Lett. **149B**, 117 (1984).

[33] P. Svrcek and E. Witten, Axions in string theory, J. High Energy Phys. 06 (2006) 051.

[34] J. P. Conlon, The QCD axion and moduli stabilisation, J. High Energy Phys. 05 (**2006**) 078.

[35] B. S. Acharya, K. Bobkov, and P. Kumar, An M theory solution to the strong CP problem and constraints on the axiverse, J. High Energy Phys. 11 (2010) 105.

[36] A. Ringwald, Searching for axions and ALPs from string theory, J. Phys. Conf. Ser. **485**, 012013 (2014).

[37] M. Cicoli, M. Goodsell, and A. Ringwald, The type IIB string axiverse and its low-energy phenomenology, J. High Energy Phys. 10 (2012) 146.

[38] J. Halverson, C. Long, B. Nelson, and G. Salinas, Towards string theory expectations for photon couplings to axion-like particles, Phys. Rev. D **100**, 106010 (2019).

[39] E. Witten, Some properties of O(32) superstrings, Phys. Lett. **149B**, 351 (1984).

[40] M. B. Wise, H. Georgi, and S. L. Glashow, SU(5) and the Invisible Axion, Phys. Rev. Lett. **47**, 402 (1981).

[41] G. Ballesteros, J. Redondo, A. Ringwald, and C. Tamarit, Standard Model—axion—seesaw—Higgs portal inflation. Five problems of particle physics and cosmology solved in one stroke, J. Cosmol. Astropart. Phys. 08 (2017) 001.

[42] A. Ernst, A. Ringwald, and C. Tamarit, Axion predictions in $SO(10) \times U(1)_{PQ}$ models, J. High Energy Phys. 02 (2018) 103.

[43] L. Di Luzio, A. Ringwald, and C. Tamarit, Axion mass prediction from minimal grand unification, Phys. Rev. D **98**, 095011 (2018).

[44] A. Ernst, L. Di Luzio, A. Ringwald, and C. Tamarit, Axion properties in GUTs, Proc. Sci. CORFU2018 (**2019**) 054 [arXiv:1811.11860].

[45] P. Fileviez Pérez, C. Murgui, and A. D. Plascencia, The QCD axion and unification, J. High Energy Phys. 11 (2019) 093.

[46] P. Fileviez Pérez, C. Murgui, and A. D. Plascencia, Axion dark matter, proton decay and unification, J. High Energy Phys. 01 (2020) 091.

[47] P. Sikivie, N. Sullivan, and D. B. Tanner, Proposal for Axion Dark Matter Detection Using an LC Circuit, Phys. Rev. Lett. **112**, 131301 (2014).

[48] S. Chaudhuri, P. W. Graham, K. Irwin, J. Mardon, S. Rajendran, and Y. Zhao, Radio for hidden-photon dark matter detection, Phys. Rev. D **92**, 075012 (2015).

[49] Y. Kahn, B. R. Safdi, and J. Thaler, Broadband and Resonant Approaches to Axion Dark Matter Detection, Phys. Rev. Lett. **117**, 141801 (2016).

[50] M. Silva-Feaver, S. Chaudhuri, H.-M. Cho, C. Dawson, P. Graham, K. Irwin, S. Kuenstner, D. Li, J. Mardon, H. Moseley *et al.*, Design overview of dm radio pathfinder experiment, IEEE Trans. Appl. Supercond. **27**, 1 (2016).

[51] J. L. Ouellet *et al.*, First Results from ABRACADABRA-10 cm: A Search for Sub-μeV Axion Dark Matter, Phys. Rev. Lett. **122**, 121802 (2019).

[52] C. P. Salemi *et al.*, Search for Low-Mass Axion Dark Matter with ABRACADABRA-10 cm, Phys. Rev. Lett. **127**, 081801 (2021).

[53] A. V. Gramolin, D. Aybas, D. Johnson, J. Adam, and A. O. Sushkov, Search for axion-like dark matter with ferromagnets, Nat. Phys. **17**, 79 (2021).

[54] N. Crisosto, P. Sikivie, N. S. Sullivan, D. B. Tanner, J. Yang, and G. Rybka, ADMX SLIC: Results from a Superconducting LC Circuit Investigating Cold Axions, Phys. Rev. Lett. **124**, 241101 (2020).

[55] J. Ouellet *et al.*, Probing the QCD axion with DMRadio-m^3, Snowmass 2021 Letter of Interest, https://www.snowmass21.org/docs/files/summaries/CF/ SNOWMASS21-CF2_CF 0-IF1_IF0_Ouellet-217.pdf.

[56] L. Brouwer *et al.* (DMRadio Collaboration), DMRadio-m^3: A search for the QCD axion below 1 μeV, Phys. Rev. D **106**, 103008 (2022).

[57] M. Dine, W. Fischler, and M. Srednicki, A simple solution to the strong CP problem with a harmless axion, Phys. Lett. **104B**, 199 (1981).

[58] D. Akerib *et al.*, The LUX-ZEPLIN (LZ) experiment, Nucl. Instrum. Methods Phys. Res., Sect. A **953**, 163047 (2020).

[59] E. Aprile *et al.* (XENON Collaboration), Dark Matter Search Results from a One Ton-Year Exposure Of XENON1T, Phys. Rev. Lett. **121**, 111302 (2018).

[60] R. Agnese *et al.* (SuperCDMS Collaboration), Results from the Super Cryogenic Dark Matter Search Experiment at Soudan, Phys. Rev. Lett. **120**, 061802 (2018).

[61] J. Ouellet and Z. Bogorad, Solutions to axion electrodynamics in various geometries, Phys. Rev. D **99**, 055010 (2019).

[62] P. F. de Salas and A. Widmark, Dark matter local density determination: Recent observations and future prospects, Rep. Prog. Phys. **84**, 104901 (2021).

[63] K. Freese, M. Lisanti, and C. Savage, Colloquium: Annual modulation of dark matter, Rev. Mod. Phys. **85**, 1561 (2013).

[64] P. Sikivie, Detection rates for "invisible"-axion searches, Phys. Rev. D **32**, 2988 (1985).

[65] S. Chaudhuri, Impedance matching to axion dark matter: Considerations of the photon-electron interaction, J. Cosmol. Astropart. Phys. 12 (2021) 033.

[66] J. L. Ouellet, C. P. Salemi, J. W. Foster, R. Henning, Z. Bogorad, J. M. Conrad, J. A. Formaggio, Y. Kahn, J. Minervini, A. Radovinsky, N. L. Rodd, B. R. Safdi, J. Thaler, D. Winklehner, and L. Winslow, First Results from Abracadabra-10 cm: A Search for Sub-μeV Axion Dark Matter, Phys. Rev. Lett. **122**, 121802 (2019).

[67] J. L. Ouellet, C. P. Salemi, J. W. Foster, R. Henning, Z. Bogorad, J. M. Conrad, J. A. Formaggio, Y. Kahn, J. Minervini, A. Radovinsky, N. L. Rodd, B. R. Safdi, J. Thaler, D. Winklehner, and L. Winslow, Design and implementation of the abracadabra-10 cm axion dark matter search, Phys. Rev. D **99**, 052012 (2019).

[68] C. P. Salemi, J. W. Foster, J. L. Ouellet, A. Gavin, K. M. W. Pappas, S. Cheng, K. A. Richardson, R. Henning, Y. Kahn,

R. Nguyen, N. L. Rodd, B. R. Safdi, and L. Winslow, Search for Low-Mass Axion Dark Matter with Abracadabra-10 cm, Phys. Rev. Lett. **127,** 081801 (2021).

[69] A. V. Gramolin, D. Aybas, D. Johnson, J. Adam, and A. O. Sushkov, Search for axion-like dark matter with ferromagnets, Nat. Physics **17,** 79 (2021).

[70] N. Crisosto, P. Sikivie, N. S. Sullivan, D. B. Tanner, J. Yang, and G. Rybka, Admx Slic: Results from a Superconducting LC Circuit Investigating Cold Axions, Phys. Rev. Lett. **124,** 241101 (2020).

[71] A. Phipps, S. E. Kuenstner, S. Chaudhuri, C. S. Dawson, B. A. Young, C. T. FitzGerald, H. Froland, K. Wells, D. Li, H. M. Cho, S. Rajendran, P. W. Graham, and K. D. Irwin, Exclusion limits on hidden-photon dark matter near 2 nev from a fixed-frequency superconducting lumped-element resonator, in *Microwave Cavities and Detectors for Axion Research*, edited by G. Carosi and G. Rybka (Springer International Publishing, Cham, 2020), pp. 139–145, 10.1007/978-3-030-43761-9_16.

[72] P. Falferi, M. Cerdonio, L. Franceschini, R. Macchietto, S. Vitale, and J. P. Zendri, A high inductance kHz resonator with a quality factor larger than 106, Rev. Sci. Instrum. **65,** 2916 (1994).

[73] H. Nagahama *et al.*, Highly sensitive superconducting circuits at ∼700 kHz with tunable quality factors for image-current detection of single trapped antiprotons, Rev. Sci. Instrum. **87,** 113305 (2016).

[74] S. Ulmer, H. Kracke, K. Blaum, S. Kreim, A. Mooser, W. Quint, C. C. Rodegheri, and J. Walz, The quality factor of a superconducting rf resonator in a magnetic field, Rev. Sci. Instrum. **80,** 123302 (2009).

[75] B. M. Brubaker, First results from the HAYSTAC axion search, Ph.D. thesis, Yale University, 2017, arXiv: 1801.00835.

[76] A. Godeke, D. Cheng, D. R. Dietderich, P. Ferracin, S. O. Prestemon, G. Sabbi, and R. M. Scanlan, Limits of NbTi and Nb₃Sn, and development of W&R Bi–2212 high field accelerator magnets, IEEE Trans. Appl. Supercond. **17,** 1149 (2007).

[77] N. Mitchell, D. Bessette, R. Gallix, C. Jong, J. Knaster, P. Libeyre, C. Sborchia, and F. Simon, The ITER magnet system, IEEE Trans. Appl. Supercond. **18,** 435 (2008).

[78] L. Bottura, G. de Rijk, L. Rossi, and E. Todesco, Advanced accelerator magnets for upgrading the lhc, IEEE Trans. Appl. Supercond. **22,** 4002008 (2012).

[79] E. Todesco *et al.*, Progress on HL-LHC Nb₃Sn magnets, IEEE Trans. Appl. Supercond. **28,** 1 (2018).

[80] H. Maeda and Y. Yanagisawa, Recent developments in high-temperature superconducting magnet technology (review), IEEE Trans. Appl. Supercond. **24,** 1 (2014).

[81] A. J. Creely *et al.*, Overview of the sparc tokamak, J. Plasma Phys. **86,** 865860502 (2020).

[82] S. Chaudhuri, K. Irwin, P. W. Graham, and J. Mardon, Optimal impedance matching and quantum limits of electromagnetic axion and hidden-photon dark matter searches, arXiv:1803.01627v3.

[83] S. Chaudhuri, K. D. Irwin, P. W. Graham, and J. Mardon, Optimal electromagnetic searches for axion and hidden-photon dark matter, arXiv:1904.05806.

[84] K. M. Backes *et al.*, A quantum enhanced search for dark matter axions, Nature (London) **590,** 238 (2021).

[85] A. V. Dixit, S. Chakram, K. He, A. Agrawal, R. K. Naik, D. I. Schuster, and A. Chou, Searching for Dark Matter with a Superconducting Qubit, Phys. Rev. Lett. **126,** 141302 (2021).

[86] C. M. Caves, Quantum limits on noise in linear amplifiers, Phys. Rev. D **26,** 1817 (1982).

[87] A. A. Clerk, M. H. Devoret, S. M. Girvin, F. Marquardt, and R. J. Schoelkopf, Introduction to quantum noise, measurement, and amplification, Rev. Mod. Phys. **82,** 1155 (2010).

[88] P. Falferi, M. Bonaldi, M. Cerdonio, R. Mezzena, G. A. Prodi, A. Vinante, and S. Vitale, 10ℏ superconducting quantum interference device amplifier for acoustic gravitational wave detectors, Appl. Phys. Lett. **93,** 172506 (2008).

[89] J. Clarke and A. I. Braginski, *The SQUID Handbook: Applications of SQUIDs and SQUID Systems* (John Wiley & Sons, New York, 2006).

[90] J. Clarke, C. D. Tesche, and R. P. Giffard, Optimization of DC SQUID voltmeter and magnetometer circuits, J. Low Temp. Phys. **37,** 405 (1979).

[91] N. S. Kampel, R. W. Peterson, R. Fischer, P.-L. Yu, K. Cicak, R. W. Simmonds, K. W. Lehnert, and C. A. Regal, Improving Broadband Displacement Detection with Quantum Correlations, Phys. Rev. X **7,** 021008 (2017).

[92] S. Chaudhuri, The dark matter radio: A quantum-enhanced search for QCD axion dark matter, Ph.D. thesis, Stanford University, 2019.

[93] S. E. Kuenstner, E. C. van Assendelft, S. Chaudhuri, H.-M. Cho, J. Corbin, S. W. Henderson, F. Kadribasic, D. Li, A. Phipps, N. M. Rapidis *et al.*, Quantum metrology of low frequency electromagnetic modes with frequency upconverters, arXiv:2210.05576.

[94] S. Kuenstner *et al.*, Optimizing frequency upconverters for quantum metrology of low frequency electromagnetic modes (to be published).

[95] P. Krantz, M. Kjaergaard, F. Yan, T. P. Orlando, S. Gustavsson, and W. D. Oliver, A quantum engineer's guide to superconducting qubits, Appl. Phys. Rev. **6,** 021318 (2019).

[96] B. Abbott *et al.*, Observation of a kilogram-scale oscillator near its quantum ground state, New J. Phys. **11,** 073032 (2009).

[97] M. Aspelmeyer, T. J. Kippenberg, and F. Marquardt, Cavity optomechanics, Rev. Mod. Phys. **86,** 1391 (2014).

[98] A. A. Clerk, F. Marquardt, and K. Jacobs, Back-action evasion and squeezing of a mechanical resonator using a cavity detector, New J. Phys. **10,** 095010 (2008).

[99] M. A. Castellanos-Beltran, K. D. Irwin, G. C. Hilton, L. R. Vale, and K. W. Lehnert, Amplification and squeezing of quantum noise with a tunable josephson metamaterial, Nat. Phys. **4,** 929 (2008).

[100] O. Hosten, N. J. Engelsen, R. Krishnakumar, and M. A. Kasevich, Measurement noise 100 times lower than the quantum-projection limit using entangled atoms, Nature (London) **529,** 505 (2016).

[101] A. Romanenko, R. Pilipenko, S. Zorzetti, D. Frolov, M. Awida, S. Belomestnykh, S. Posen, and A. Grassellino, Three-dimensional superconducting

resonators at $T < 20$ mK with the photon lifetime up to $\tau = 2$ seconds, Phys. Rev. Appl. **13**, 034032 (2020).

[102] D. Blair and S. Jones, Highqsapphire loaded superconducting cavities and application to ultrastable clocks, IEEE Trans. Mag. **21**, 142 (1985).

[103] E. J. Daw, Resonant feedback for axion and hidden sector dark matter searches, Nucl. Instrum. Methods Phys. Res., Sect. A **921**, 50 (2019).

[104] H. W. Bode, *Network Analysis and Feedback Amplifier Design* (D. van Nostrand, New York, NY, 1945).

[105] R. Fano, Theoretical limitations on the broadband matching of arbitrary impedances, J. Franklin Inst. **249**, 57 (1950).

[106] S. E. Sussman-Fort and R. M. Rudish, Non-foster impedance matching of electrically-small antennas, IEEE Trans. Antennas Propag. **57**, 2230 (2009).

[107] M. Salit and M. S. Shahriar, Enhancement of sensitivity and bandwidth of gravitational wave detectors using fast-light-based white light cavities, J. Optics **12**, 104014 (2010).

[108] A. Shlivinski and Y. Hadad, Beyond the Bode-Fano Bound: Wideband Impedance Matching for Short Pulses Using Temporal Switching of Transmission-Line Parameters, Phys. Rev. Lett. **121**, 204301 (2018).

[109] Snowmass community, Snowmass2021 Cosmic Frontier White Paper: Magnet Development, Contribution to Snowmass 2021 (to be published).

[110] S. Awaji, K. Watanabe, H. Oguro, H. Miyazaki, S. Hanai, T. Tosaka, and S. Ioka, First performance test of a 25 t cryogen-free superconducting magnet, Supercond. Sci. Technol. **30**, 065001 (2017).

[111] S. Hahn, K. Kim, K. Kim, X. Hu, T. Painter, I. Dixon, S. Kim, K. R. Bhattarai, S. Noguchi, J. Jaroszynski, and D. C. Larbalestier, 45.5-tesla direct-current magnetic field generated with a high-temperature superconducting magnet, Nature (London) **570**, 496 (2019).

[112] R. Kolb, H. Weerts, N. Toro, R. Van de Water, R. Essig, D. McKinsey, K. Zurek, A. Chou, P. Graham, J. Estrada *et al.*, *Basic Research Needs for Dark-Matter Small Projects New Initiatives: Report of the Department of Energy's High Energy Physics Workshop on Dark Matter*, Technical Report (USDOE Office of Science (SC) (United States), 2018).

[113] M. S. Turner, Periodic signatures for the detection of cosmic axions, Phys. Rev. D **42**, 3572 (1990).